

Long-range structural fluctuations in a $\text{CaO-Al}_2\text{O}_3\text{-2SiO}_2$ glass observed by spatially resolved near-edge spectroscopy

Nan Jiang*

Department of Physics and Astronomy, Arizona State University, Tempe, Arizona 85287-1504

Jianrong Qiu

Photon Craft Project, Shanghai Institute of Optics and Fine Mechanics, Chinese Academy of Sciences, Shanghai 201800, China

John C. H. Spence

Department of Physics and Astronomy, Arizona State University, Tempe, Arizona 85287-1504

(Received 26 March 2002; published 14 August 2002)

We report evidence for long-range structural fluctuations in a $\text{CaO-Al}_2\text{O}_3\text{-2SiO}_2$ glass of homogeneous composition. Our new experimental method is based on spatial variations in the electron energy-loss near-edge spectroscopy (ELNES), using the small focused probe of an electron microscope. The results are obtained from the average of the short to medium-range structures around Al and Si, which are obtained by comparing experimental data in the glass with calculations of the local density of states in a compositionally equivalent (anorthite) crystal.

DOI: 10.1103/PhysRevB.66.054203

PACS number(s): 61.43.Fs; 79.20.Uv; 71.20.Ps

I. INTRODUCTION

The structural characterization of glasses is essential to any adequate understanding of their properties. After several decades of effort, however, the application of microstructural knowledge to macroscopic physical and chemical properties of glasses has rarely been successful, probably because of our limited structural knowledge, compared to that of crystal structures.¹ In general, a glass is considered to be a random structure, but below a certain length scale, deviations from randomness can be seen. For example, in silicate glasses, the evidence for short-range structure (at the nearest-neighbor distance) around Si is overwhelming, and the coordination of Al is also conclusive.² The definition of medium-range structures (from second nearest neighbor distance to 1.0 to 2.0 nm), however, is more contentious.³ The strongest evidence for the existence of medium-range structures in silicate glasses comes from measurements of well-defined local environments (nearest neighbors) around species (alkali and alkaline earth cations) with weak, ionic bonds to oxygen.^{4,5,6} However, the nature of the medium-range structure in these glasses is still not clear. Recently, medium-range structural fluctuations have been revealed by fluctuation electron microscopy in as-deposited amorphous semiconductor thin films.⁷ However, there remains little structural information beyond the upper limit of medium-range structure. Deviations from randomness in the long-range structure are normally considered to be compositional.

There are two extreme models for the structure of glasses: random networks and microcrystallite models. Historically, random networks have been considered to be the most appropriate models. Random networks are likely to be the lowest energy state of amorphous tetrahedral semiconductors,⁸ but not for many oxide glasses. More flexible models, the stereochemically defined (SCD) models, have been proposed, which cover the spectrum from continuous random networks to microcrystallite models.⁹ No matter which ap-

proach is favored, however, the structure is always homogeneous on average (over length scales greater than about 1–2 nm). In this study, we use a spatially resolved spectroscopic method to demonstrate the existence of structural fluctuation in the long-range structure of a compositionally homogeneous $\text{CaO-Al}_2\text{O}_3\text{-2SiO}_2$ (anorthite) glass.

The long-range structure is deduced from the average of the short to medium-range structure around Al and Si, which are obtained by comparing electron energy-loss spectra (EELS) in the glass with calculations of the density of states (DOS) in a compositionally equivalent single crystal. The local structures in Ca aluminosilicate glasses have been the subject of intensive research.¹⁰ In particular, a comparison of glassy and crystalline anorthite phases has been published.¹¹ It is generally agreed that Si and Al are tetrahedrally coordinated to oxygen. However, the average coordination numbers of Ca-O vary from 5.2 by x-ray diffraction¹⁰ to 7 by extended x-ray absorption fine structure spectroscopy.¹¹

II. THEORY

Our experimental approach is based on EELS with moderate spatial resolution in a transmission electron microscope (TEM). The near-edge fine structure of EELS (ELNES) is similar to that of x-ray-absorption spectra (XANES), but has the advantage of much higher spatial resolution. In a single particle description, EELS is due to the primary (incident) electrons' interaction with inner-shell electrons, and the energy required to excite the core electron of the atom from the initial state to an unoccupied final state. As derived from Fermi's golden rule, the EELS spectrum is proportional to the unoccupied DOS $[\rho(E)]$ modified by the atomic transition matrix element $|M(q,E)|^2$,^{12,13}

$$I(E,q) \propto |M(q,E)|^2 \cdot \rho(E),$$

where q is the wave vector. If the collection aperture is small ($\mathbf{q} \cdot \mathbf{r} \ll 1$), dipole selection rule applies; therefore the EELS intensity can be simplified as

$$I(E, q) \propto |M_{l+1}|^2 \rho_{l+1}(E) + |M_{l-1}|^2 \rho_{l-1}(E),$$

where l is the angular-momentum quantum number of the initial state. For Al and Si L edges excited by 100 keV electrons, the dipole selection rule is fulfilled in the near edge region if the collection aperture is smaller than 10–11 mrad.¹⁴ To a first approximation, $|M_{l\pm 1}|^2$ only represents the overall shape of the edges without fine structure.¹⁵ Neglecting the matrix element, the ELNES can be directly compared to the partial DOS, restricted by the dipole selection rule. If the initial state consists of a deep core level, which is highly localized, then $\rho_{l\pm 1}(E)$ becomes the local density of states (LDOS). Therefore the ELNES is sensitive to the local structure.¹⁶ In this study, the L -edge ELNES is used to observe the local structure around Al and Si in a CaO-Al₂O₃-2SiO₂ glass using a 50 nm diameter electron probe. The s and d -LDOS were calculated to interpret the experimental data.

The LDOS were calculated using the real-space multiple-scattering-theory method.¹⁷ The calculations were carried out using the code FEEF8.¹⁸ As an extension to previous versions of FEEF codes, FEEF8 uses self-consistent-field (SCF) muffin-tin potentials. It is noted that the strong interaction between the electron and core hole can modify the final state drastically.¹⁹ Therefore ground state DOS calculations can fail to interpret EELS in many cases.²⁰ In this study, the core-hole effect is represented using the final state approach, which is the one with an electron in the unoccupied state, and a hole in the atomic core.²¹ Many-body effects are ignored in the calculations.

III. EXPERIMENT

Two samples of glassy and crystalline anorthite were studied. The glass preparations followed the standard procedure. The CaO-Al₂O₃-2SiO₂ batch was mixed in a platinum crucible and melted in an electric furnace at 1550 °C for one hour under an ambient atmosphere. The glass samples were obtained by quenching the melt to room temperature. Anorthite crystal samples were obtained by annealing the glass samples at 1000 °C for 2 h. The match of the x-ray diffraction intensities with a standard anorthite sample confirms the crystal structure. (Only a broad peak was observed in the glass samples.) Electron microscope specimens were prepared by picking up tiny pieces of glass or crystals suspended in acetone using a holey carbon film across a copper grid. An advantage of this method is that there is less contamination on the surfaces. The specimens were observed in a Philips EM400 with a field-emission gun and a Gatan parallel EELS system. The energy resolution of the spectrometer is about 0.8 eV. Each spectrum has been deconvoluted from the zero-loss spectrum using the Fourier-log method.²² Backgrounds were fitted at pre-edge intensities using an exponential form, and subtracted from the deconvoluted raw data. The origin of the energy axis is set at zero where the maximum intensity of the zero-loss peak occurs. Since a 0.2 eV

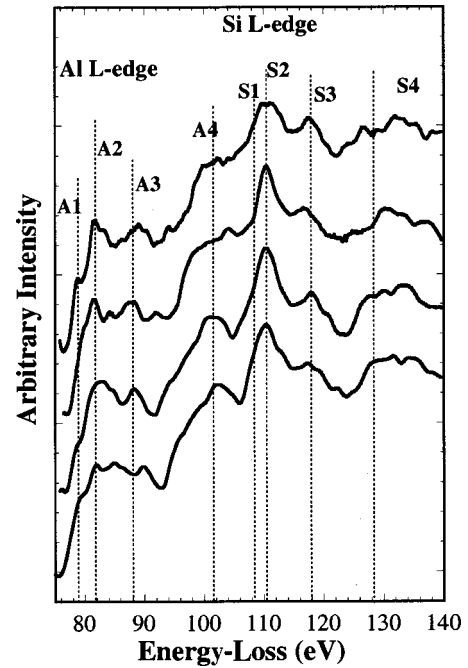


FIG. 1. Experimental EELS spectra from different areas in the glass. Vertical lines are guides for the eyes.

energy window was selected, there is ± 0.2 eV uncertainty in the energy scale.

IV. RESULTS AND DISCUSSION

Figure 1 shows Al L and Si L ELNES spectra recorded from four different regions. The experimental conditions (electron beam current, energy window, etc.) are the same, although the thickness may vary. Specimen thickness can be simply estimated in terms of the effective mean-free-path for inelastic scattering, λ , using the log-ratio method,²³ $t/\lambda = \ln(I_t/I_0)$, where I_t and I_0 are the EELS intensities under the whole spectrum and under the zero-loss peak, respectively. In four different regions, t/λ is successively equal to 0.51, 0.53, 0.43, and 0.48 (from top to bottom). Approximately, the above four regions have similar thickness. Taking the value of λ (~ 120 nm) in amorphous SiO₂, the estimated thicknesses are 61, 64, 53, and 58 nm, respectively. To reduce radiation damage, the illuminated areas were broadened to about 50 nm \times 50 nm. It should be noted that silicate glasses are very sensitive to electron irradiation. In a previous study, we have shown that the initial damage in a Ca aluminosilicate glass occurs when the Ca is removed from its site by electron irradiation.²⁴ Therefore changes in the intensity of the Ca M_{23} edge, which is around 33 eV, was used as a criterion for damage. In each region, time-resolved spectra were recorded; the acquisition time for each spectrum is 0.05 s. Those spectra for which the intensity of the Ca M_{23} edge did not change were added together to give the spectra in Fig. 1, while those for which the Ca intensity changed were discarded. The total acquisition times for the spectra in Fig. 1 vary from 1.4 to 1.5 s.

It is seen that the overall features in the Al L and Si L ELNES recorded from different regions are similar. There

are four distinguishable features (A1, A2, A3, and A4) in the Al *L* ELNES and three (S2, S3, and S4) in the Si *L* ELNES. However, the details vary from spectrum to spectrum. The intensities of peak A1 are significantly different although their positions are same (at ~78 eV). The shapes of peak A2 all look different in those spectra: sharp in the first two areas but broad in the others. The positions of peak A3 vary from 88 to 90 eV. The appearance of peak A4 is also different. The differences also occur in the Si *L* ELNES. However, it is difficult to separate the Si ELNES from the tails of the Al *L* edges.

Phase separation is not observed visually from TEM images. Composition fluctuations in the above regions can also be ignored since the variations of cation intensity ratios are very small. The ratios of the EELS intensity of the Ca *M*₂₃ edges in the different regions ($I_{Ca}^1:I_{Ca}^2:I_{Ca}^3:I_{Ca}^4 = 1:7.71:1.86:1.37$) are approximately equal to those of the Al *L*₂₃ edges ($I_{Al}^1:I_{Al}^2:I_{Al}^3:I_{Al}^4 = 1:7.65:1.83:1.37$). The intensity ratios of the Si *L*₂₃ edge including the background from the tails of the Al *L*₂₃ edge, to the Al *L*₂₃ edge, ($(I_{Si}/I_{Al})^1:(I_{Si}/I_{Al})^2:\dots = 2.30:2.22:2.35:2.47$) are also similar in the different areas. Therefore, the glass can be considered to be compositionally homogeneous. The differences in the ELNES must therefore be due to changes in the local structure.

Comparison with a compositionally equivalent crystal may show some correspondence between characteristic features for crystal and glass. The Al and Si *L* edges in an anorthite crystal are shown in Fig. 2; these were obtained under the same experimental conditions as those in the glass. Channeling orientations were carefully avoided. The detailed features in the crystal do not change with the observed regions. It is seen that the overall features in the crystal are similar to those in the glass; subpeaks A1, A2, A3, and A4 in the Al *L* ELNES and S2, S3, and S4 in the Si *L* all appear in the spectrum. However, the details are also slightly different from those observed in the glass. The interpretation of these subpeaks can be obtained by comparing the experimental ELNES with the LDOS calculations for the anorthite crystal structure. The calculated final states (including core-hole effects) are also plotted in Fig. 2, aligned to the major peaks in the experimental spectrum. Restricted by the dipole selection rule, only *s* and *d* components and their sum are presented. In general, the calculated LDOS peaks agree with those of the experimental EELS very well. For Al, peak A2 is dominated by the Al *s* LDOS, while others features are due to the Al *d* states. For Si, both Si *s* and *d* components have peaks at the position of peak S2, while other features are from the Si *d* states. Including the core hole effects in calculations significantly sharpens the *s* components of the Al and Si, and increases the densities of the *d* components at the lower energy region.

The triclinic unit cell of anorthite contains 104 atoms, and both Al and Si have eight inequivalent sites in the unit cell, respectively.²⁵ Therefore the LDOS on Al and Si are the average over these inequivalent sites, respectively. Table I lists the bond distance distributions around inequivalent Al atoms. In anorthite, all the Al and Si are tetrahedrally coordinated with oxygen atoms. Although the Si-O distances lie

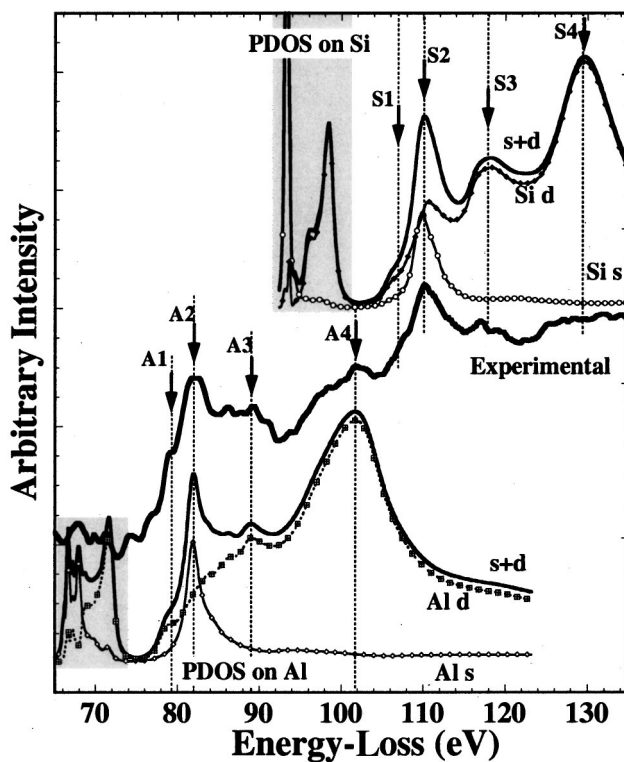


FIG. 2. Comparison of experimental EELS spectrum (thick line) of the anorthite crystal with MS calculations of LDOS (thin lines). For comparison, the energy of LDOS is scaled to the axis of energy loss. That is the lowest energy of unoccupied states corresponding to the threshold energy of EELS. The shaded areas represent occupied states. The cluster is 1 nm in radius.

between 1.60 and 1.63 Å in the SiO₄ tetrahedra, and the Al-O ranges between 1.69 and 1.82 Å in AlO₄, the first shell calculations on all inequivalent atoms of the same species give almost identical spectra. (Calculated results are not shown here.) Such nearest neighbor order determines the overall shape of the spectra, without many details in the ELNES. In Table I, the shortest Al-Si, Al-Ca, and Al-Al distances are also listed. Although variations exist, the differences are not significant. In fact, these cations themselves have very small effects on the details of the Al *L* ELNES. On the contrary, the scattering from the oxygen atoms in the second and higher nearest neighbors significantly modifies the fine structure. In the last column of Table I, we see that the distributions of O above the second nearest neighbor are divergent among the inequivalent Al atoms. Therefore, we expect a completely different appearance of the LDOS on each inequivalent Al site.

Figure 3 shows multiple scattering calculations of the LDOS on the eight inequivalent Al atoms in the anorthite crystal. It is seen that the differences in the details are significant. Some differences are big enough to affect the ELNES of the Al *L* edge. For example, peak A2 would be broad if we could only probe the Al (1) or Al (2) site; it would be very sharp if we could probe the Al (3) or Al (4) sites, and the flat A2 could be seen at the Al (5) site. Therefore, the differences in the second and higher nearest neighbors have significant effects on the details of the ELNES. This can be

TABLE I. Bond length distributions of each inequivalent Al atom in the crystal anorthite. $d_{\langle\text{Al-O}\rangle}$, $d_{\langle\text{Al-Si}\rangle}$, and $d_{\langle\text{Al-Ca}\rangle}$ are the average distances (\AA). The values in the parentheses are the coordination number.

	$d_{\langle\text{Al-O}\rangle}$	$d_{\langle\text{Al-Si}\rangle}$	$d_{\langle\text{Al-Ca}\rangle}$	$d_{\langle\text{Al-Al}\rangle}$	$d_{\text{Al-O}} (>2\text{nd})$
Al (1)	1.74 (4)	3.09 (4)	3.24 (2)	3.80 (1)	3.12, 3.45, 3.63, 3.64, ...
Al (2)	1.73 (4)	3.09 (4)	3.26 (2)	3.79 (1)	3.18, 3.33, 3.53, 3.57, ...
Al (3)	1.74 (4)	3.17 (4)	3.60 (2)	3.80 (1)	3.56, 3.63, 3.66, 3.71, ...
Al (4)	1.74 (4)	3.19 (4)	3.75 (3)	3.79 (1)	3.63, 3.65, 3.66, 3.67, ...
Al (5)	1.74 (4)	3.11 (4)	3.62 (2)	4.09 (1)	3.31, 3.47, 3.56, 3.63, ...
Al (6)	1.75 (4)	3.07 (4)	3.56 (3)	4.09 (1)	3.19, 3.34, 3.55 (2), ...
Al (7)	1.74 (4)	3.08 (4)	3.66 (3)	3.86 (1)	3.41, 3.47, 3.53, 3.61, ...
Al (8)	1.74 (4)	3.10 (4)	3.88 (3)	3.86 (1)	3.44, 3.51, 3.53, 3.54, ...

interpreted as a longer inelastic mean free path ($>10 \text{\AA}$) at low kinetic energies ($<20 \text{ eV}$) of the ejected core electron.²⁶ The excited electron propagates outwards, and is scattered by the neighboring atoms, which modifies the absorption coefficient due to the interference between the outgoing and scattered wave functions.²⁷

In crystals, the specific features of each inequivalent Al (and Si) atom contribute equally to the Al (and Si) ELNES under nonchanneling conditions; therefore the average of the LDOS on these inequivalent atoms is sufficient to explain the ELNES in the crystal (see Fig. 2). However, the “inequivalent” Al or Si sites are not necessarily evenly distributed (or even all exist) in the compositionally equivalent glass. Therefore, fluctuations in the long-range structure, if it exists, can be detected by EELS with moderate spatial resolution.

Comparing the experimental EELS in the glass with the LDOS calculations, for example, the peaks in the first spec-

trum in Fig. 1 show considerable similarity to those in the calculated LDOS on the Al (1) site (Fig. 3), while the last spectra are similar to the LDOS on the Al (6) site. Although it is difficult to say what this means, it is certain that the average structure around the Al are different in these different areas. The calculations show that the fine structure in the LDOS is only sensitive to the surrounding atoms within a radius of $\sim 2 \text{ nm}$. Those far away from the central atom have insignificant effect on the LDOS, and thus on the fine structure of the EELS. In our experiments, however, the illumination volume is much larger, about $50 \times 50 \times 50 \text{ nm}^3$. Therefore it is reasonable to suggest that long-range structural fluctuations exist in this $\text{CaO-Al}_2\text{O}_3\text{-}2\text{SiO}_2$ glass. These results imply that aluminosilicate glasses may not be an ideally random-packed structure. Application of the SCD model also therefore requires extra constraints, such as the selection of “structure forming” operations.

One of the reasons for solving glass structures is to construct atom coordinates in real-space, and to compute its macroscopic properties. Conceptually, however, it is difficult to describe glass structures when we obtain different structures from different areas. Statistical models seem necessary, such as the use of the autocorrelation function. Therefore, an extensive study of structural fluctuations at the long-range level becomes very important. We note that use of the EELS technique to solve structures is not straightforward. The real-space distribution of atoms cannot directly be extracted from the data. Theoretically, the local structure in the glass can be characterized by comparing experimental data with calculated EELS spectra computed from trial structures. In practice, this comparison is not impossible, in view of the excellent agreement now possible in ELNES calculations for known structures. However, the experimental challenge for this approach is to achieve much higher spatial resolution. ELNES with atomic-level spatial resolution has been demonstrated for semiconductors using field emission sources,²⁸ but for glasses, electron radiation damage is a major concern, and high electron beam currents must be avoided. This problem can be addressed by use of an ultrasensitive electron spectrometer, based, for example, on an Omega filter and Image Plate recording system to allow transverse integration of spectra.

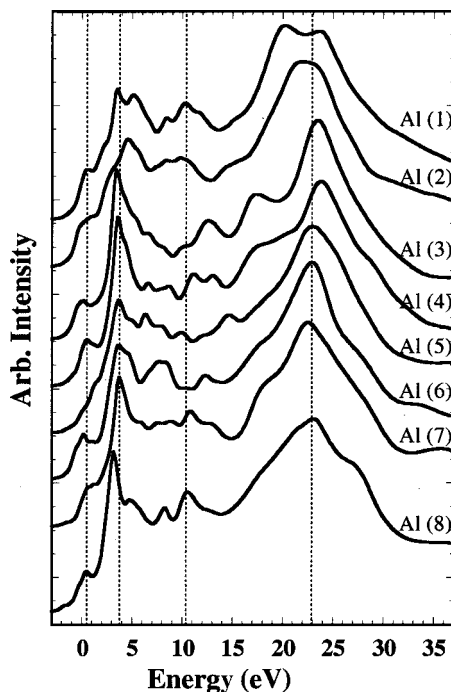


FIG. 3. MS calculations of LDOS on inequivalent Al atoms. Fermi energy is set to be zero. Vertical lines are guides for eyes.

V. CONCLUSION

In conclusion, we have presented experimental ELNES spectra of the Al and Si *L* edges in both anorthite crystals and glasses, together with multiple-scattering calculations of the LDOS on the inequivalent Al and Si atoms in the anorthite crystal. All evidence from the EELS with 50 nm spatial resolution supports the conclusion that nearest-neighbor (short-range) structure does exist in the glass. Second and higher nearest-neighbor structures (medium-range) also exist, but

may vary from area to area, resulting in structural fluctuations at the long-range level in these glasses.

ACKNOWLEDGMENTS

This work was supported by NSF Grant No. DMR9973894 (JCHS P.I.). J.Q. acknowledges the financial support from the National Natural Science Foundation of China (Grant No. 50125208).

*Corresponding author. Email address: nan.Jiang@asu.edu

¹For a review and references see P. H. Gaskell, in *Materials Science and Technology: a Comprehensive Treatment*, edited by R. W. Cahn, P. Hassen, and E. J. Kramer (VCH, Weinheim, 1991), Vol. 9, pp. 175–278.

²Z. Wu, C. Romano, A. Marcelli, A. Mottana, G. Cibin, G. D. Ventura, G. Giuli, P. Courtial, and D. B. Dingwell, *Phys. Rev. B* **60**, 9216 (1999).

³S. R. Elliott, *Nature (London)* **354**, 445 (1991).

⁴G. N. Greaves, A. Fontaine, P. Lagarde, D. Raoux, and S. J. Gurman, *Nature (London)* **293**, 611 (1981).

⁵P. H. Gaskell, M. C. Eckersley, A. C. Barnes, and P. Chieux, *Nature (London)* **350**, 675 (1991).

⁶I. Farnan, P. J. Grandinetti, J. H. Baltisberger, J. F. Stebbins, U. Werner, M. A. Eastman, and A. Pines, *Nature (London)* **358**, 31 (1992).

⁷M. M. J. Treacy and J. M. Gibson, *Acta Crystallogr., Sect. A: Found. Crystallogr.* **52**, 212 (1996).

⁸J. M. Gibson and M. M. J. Treacy, *Phys. Rev. Lett.* **78**, 1074 (1997).

⁹P. H. Gaskell, *J. Non-Cryst. Solids* **192&193**, 9 (1995), and references therein.

¹⁰V. Petkov, S. J. L. Billinge, S. D. Shastri, and B. Himmel, *Phys. Rev. Lett.* **85**, 3436 (2000), and references therein.

¹¹N. Binsted, G. N. Greaves, and C. M. B. Henderson, *Contrib. Mineral. Petrol.* **89**, 103 (1985).

¹²S. T. Manson, *Topics in Applied Physics* (Springer-Verlag, New York, 1978), Vol. 26, pp. 135–163.

¹³P. Rez, J. Bruley, P. Brohan, M. Payne, and L. A. J. Garvie, *Ultramicroscopy* **59**, 159 (1995), and references therein.

¹⁴D. K. Saldin and Y. Ueda, *Phys. Rev. B* **46**, 5100 (1992).

¹⁵R. D. Leapman, P. Rez, and D. F. Mayers, *J. Chem. Phys.* **72**, 1232 (1980).

¹⁶J. Taftø and J. Zhu, *Ultramicroscopy* **9**, 349 (1982).

¹⁷X.-G. Zhang and A. Gonis, *Phys. Rev. Lett.* **62**, 1161 (1989).

¹⁸A. L. Ankudinov, B. Ravel, J. J. Rehr, and S. D. Conradson, *Phys. Rev. B* **58**, 7565 (1998).

¹⁹M. M. Disko, J. C. H. Spence, O. F. Sankey, and D. Saldin, *Phys. Rev. B* **33**, 5642 (1986).

²⁰S. Mo and W. Y. Ching, *Phys. Rev. B* **62**, 7901 (2000), and references therein.

²¹J. J. Rehr and R. C. Albers, *Rev. Mod. Phys.* **72**, 621 (2000).

²²D. W. Johnson and J. C. H. Spence, *J. Phys. D* **7**, 771 (1974).

²³R. F. Egerton, *Electron Energy-Loss Spectroscopy in the Electron Microscope* (Plenum Press, New York, 1996), pp. 302–303.

²⁴N. Jiang, J. Qiu, A. Ellison, and J. Silcox (unpublished).

²⁵R. W. G. Wyckoff, *Crystal Structures*, 2nd ed. (Wiley, New York, 1963), Vol. 4, p. 447.

²⁶M. P. Seah and W. A. Dench, *Surf. Interface Anal.* **1**, 2 (1979).

²⁷D. E. Sayers, E. A. Stern, and F. W. Lytle, *Phys. Rev. Lett.* **27**, 1204 (1971).

²⁸D. A. Muller, T. Sorsch, S. Moccio, F. H. Baumann, K. Evans-Lutterodt, and G. Timp, *Nature (London)* **399**, 758 (1999).